SLIP PROCESSES AND FRACTURE IN IRON CRYSTALS

V. Pelikán [1], P. Hora [1], A. Machová [2] and M. Landa [2]
[1] CDM-Institute of Thermomechanics AS CR, Pilsen, 301 14 Veleslavínova 11
[2] Institute of Thermomechanics AS CR, Prague 8, 182 00 Dolejškova 5
pelikan@cdm.it.cas.cz, hora@cdm.it.cas.cz, machova@it.cas.cz, ml@it.cas.cz

ABSTRACT

We present results of 3D molecular dynamic simulations in bcc single crystals with embedded cracks of different orientations. The cracks are loaded in tension mode I. Our contribution shows that the temperature, crack orientation and various slip processes at the crack front may have different consequences for crack stability in bcc iron. The results are compared with continuum models, experimental observations and our previous plane strain simulations.

Introduction

The brittle-ductile behavior of cracks has long been an area of intensive study. In particular, the bcc iron has been studied often in the recent past in the framework of continuum (e.g. Rice *et. al.* [1-3]) and atomistic models (e.g. Mullins *et. al.* [4-8]), and as well in experiments (e.g. March *et. al.* [9], Šmida and Bošanský [[10], Landa *et. al.* [11]). The models consider usually plane strain conditions (2D) along the crack front and temperature of 0 K. However, free sample surface (where plane stress conditions are expected in the normal direction) may influence the ductile-brittle behavior, as well as the thermal atomic motion. Such studies require 3D atomistic simulations.

This paper is devoted to crack simulations by molecular dynamic (MD) technique in 3D bcc iron crystals. We use our new MD codes for parallel processing in MPI and also classical single processing. Interatomic interactions in bcc iron are described using an N-body potential of Finnis-Sinclair type from [12]. The 3D codes have been tested in perfect samples under simple uni-axial tension and in thermal simulations. The simulated thermal expansion in bcc iron agrees well with experimental data [13], as well as the phonon frequency spectra [12].

In the present work, two different crack orientations (crack plane/crack front) are treated: a pre-existing Griffith (through) **central crack (001)[010**] and an **edge crack (001)[110**] (through, pre-existing). The relatively long cracks are embedded in **thin** bcc iron crystals of different orientations and loaded in tension **mode I.** The simulations with the edge (001)[110] crack have been motivated by our fracture experiments [11] on Fe-Si(3wt%) single crystals with edge crack performed at room temperature and thus, the 3D-simulations were performed only at temperature of 300 K. The simulations with the Griffith central crack have been performed at temperature of 0 K and 300 K to see the influence of temperature on the brittle-ductile behavior.

MD simulations

Interatomic interactions across free crack faces of the initial pre-existing cracks are not allowed. Surface relaxation has been performed before a loading to avoid its influence on crack tip processes. The samples were loaded symmetrically in the <001> directions by prescribing external forces F_{ext} distributed homogeneously at individual atoms lying in several surface layers, similar to [7]. Newtonian equations of motion for the individual atoms have been solved by a central difference method using time integration step $h = 1\text{x}10^{-14}$ s. Each time step $t = n\,h$ we monitored the total number of existing interactions and global energy balance in the system.

Central (001)[010] crack

The crystal with basic cubic orientation {100} consists of 1999 planes in the [100] direction, 100 planes along the crack front in the [010] direction and 1999 planes in the [001] direction. The central pre-existing (through) crack has been placed in the middle of the crystal. The crack is introduced by removing part of atoms from the central (001) plane. The initial half crack length in the [100] direction is $l_o = 100\ a_o$, where $a_o = 2.8665$ Å is the lattice parameter. The initial half crack opening is $c_o = a_o$. The total number of atoms in the crystal is $N = 98\ 892\ 298$. Parallel processing in MPI has been used for these simulations.

The initial atomic velocities at temperature of 0 K were zero (i.e. $E_{kin}(0) = 0$ in the system) and the further thermal atomic motion has not been controlled. The crystal was loaded with external forces gradually (linearly) according to scheme in Figure 1 for 0 K. Crack initiation has been monitored shortly after time step 23000 and thus, the simulations were stopped at time step 24000.

In simulations at temperature of 300 K, the crystal was heated gradually by prescribing random atomic velocities, until the average kinetic energy in the system $\bar{E}_{kin} = 3/2\ k_B\ \bar{T}\ N$ corresponded to the average temperature $\bar{T} = 300$ K (here k_B is the Boltzmann constant). When this steady state was reached, the crystal has been loaded gradually with the same loading rate as described above. When the slip processes and slow plastic crack growth were detected, the external forces have been kept at a constant level from the time step 16514 - see Figure 1.

The crack tip processes in 3D were visualized initially along the crack front, i.e. in the atomic planes of the type {010}, perpendicular to the crack front. It enabled us to observe a crack advance and also some shear processes along the crack front. In addition, at temperature of 300 K we have been visualized the shear processes also in {110} and {112} slip planes. To recognize the slip patterns coming from the different slip planes, we have been performed also "block like shear" (BLS) simulations in 3D perfect bcc iron crystals. During these simulations, the crystal is divided in two parts: one part is fixed and the second part is shifted (displaced) gradually as a rigid body along a plane {110} or {112} in the slip direction <111> by the *Burgers vector* $\boldsymbol{b} = a_o/2$ <111>.

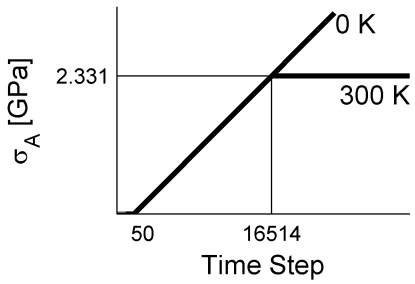

Figure 1. Scheme of loading at temperature of 0 K and 300 K. [14]

Edge (001)[110] crack

The simulated crystal has the same orientation and similar geometry as in the fracture experiments [11]: the edge crack lies on a (001) plane, crack front is oriented along the [110] direction and the direction of potential crack extension is [-110]. The crystal contains 600 planes (001) (along the length L), 100 planes (-110) (along the width W) and 20 planes (110) along the crack front (thickness B). The initial edge crack of the length $l_o = 30\ a_o / \sqrt{2}$ was placed in the middle of the crystal and it was created by cutting of interatomic bonds across the crack plane. Half of the initial crack opening is $c_o = a_o / 4$. The ratio l_o/W (crack length vs. sample width) and the boundary correction factor $F_I = 1.27$ are similar in simulations and in experiments according to linear fracture mechanics (LFM). We have verified that distribution of external forces at the sample borders satisfy the constant displacements conditions at the loaded borders, similar to the experiment. The simulated crystal was initially heated up to average temperature of 300 K during 1000 time steps. After that, the crystal was gradually (linearly) loaded during 3200 time steps up to an applied stress level of 8.42 GPa. The crack advance and slip processes have been monitored along the crack front, i.e. in individual {110} planes, perpendicular to the crack front. The total number of atoms in the system is $N = 600000$ and single processing has been used in this case.

Results and discussions

Beside the stress and temperature, the microscopic processes at the crack front depend on the mutual orientation of the crack and accessible slip systems (see e.g. [4-8], [15-16]) and so, we will discuss the two different crack orientations separately. Our cracks are relatively long and the ratio $l_o / c_o > 20$, i.e. according to our Goodier analysis for elliptical cracks (see also [17]), the cracks are sufficiently narrow and thus, stress concentration at the crack can be treated according to fracture mechanics [18].

Central (001)[010] crack

Figure 2 displays lateral contraction (i.e. the strain component ε_z) along the crack front at temperature of 0 K in elastic region of loading. Figure shows that at the left and right corners (where the crack front penetrates perpendicularly the free sample surfaces), the contraction is large to obey the plane stress conditions at the free surfaces. The contraction is significant also in the middle, i.e. the stress state in the middle of our **thin crystals** is neither plane stress ($\sigma_z = 0$) and nor plane strain ($\varepsilon_z = 0$), but something between, as Figure 2 indicates.

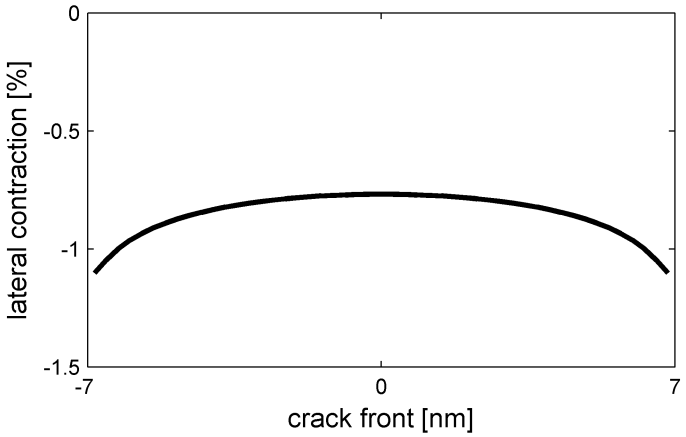

Figure 2. Lateral contraction along the left crack front; time step 8000, 0 K. [14]

At temperature of 0 K we observed brittle crack initiation at time step 23340 in the middle of the crystal. Since the crystal is relatively large in the direction of loading, flight time correction [5] for the loading waves should be included to estimate the stress intensity at the crack plane placed in the middle of the crystal. Using the elastic constants for our potential from [12], the flight time correction corresponds to 2582 time steps, which reduces the value of the applied stress in the middle to 2.93 GPa and the stress intensity to K_I = 0.879 MPa $m^{1/2}$. The K_I from MD exceeds only slightly the critical Griffith stress intensity expected according to anisotropic LFM for cleavage mechanism of crack initiation: K_G = 0.817 MPa $m^{1/2}$ for plane strain, K_G = 0.793 MPa $m^{1/2}$ for plane stress. Shortly after crack initiation the simulation at the temperature of 0 K has been stopped, as already mentioned above.

At elevated temperature of 300 K, two different slip patterns have been observed at the crack front. The patterns more close to the crack tip were inclined to the crack front under an angle $\theta \approx 45^o$, the different patterns at larger distance from the crack tip deviated from the original direction. We have verified by means of block like shear simulations (described in the previous section) that the patterns under the angle 45^o at the crack tip come from the slip processes on {101} planes. The deviated second patterns come from the slip processes on {112} planes that lies under the angle $\theta = 26.565^o$ with respect to the crack plane.

The two available slip systems at the left crack front are shown schematically in Figure 3. The slip system (101)[-1-11] is inclined to the crack plane and contains the crack front. Dislocation emission in this slip system results in the two crystalline block being shifted in the direction of Burgers vector ***b***, which causes crack tip blunting (Figure 4b). The second slip system (112)[-1-11] is oblique to the crack front and dislocation emission makes a jog in the crack front in the direction of ***b*** (Figure 4a).

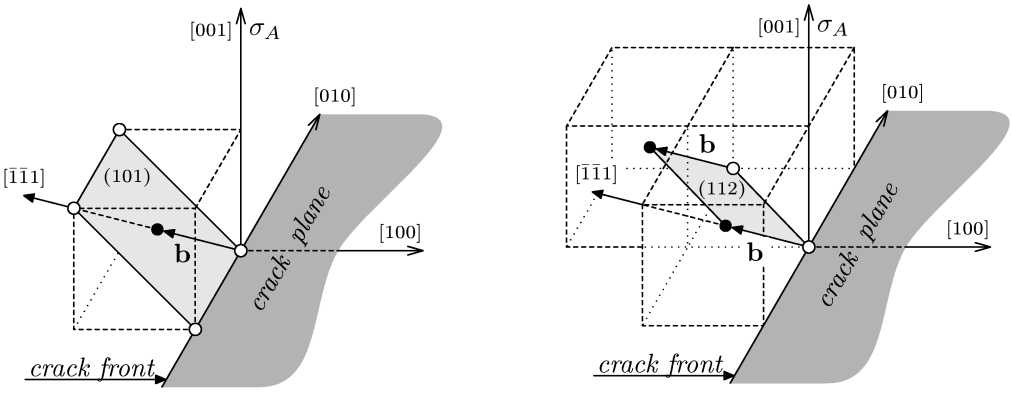

Figure 3. Scheme of the slip planes at the left crack front.

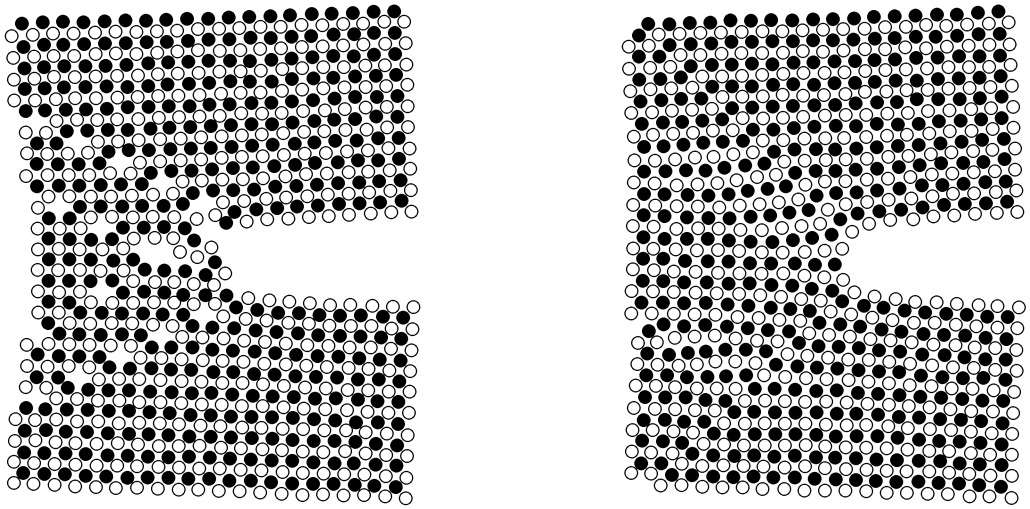

Figure 4. Slip patterns in the middle of the crystal coming from the <-1-11>{112} slip systems (a). Crack blunting close to the free surface due to dislocation emission on {101} planes (b). Time step 15820, 300 K, view (010)[010]. [14]

We have found that plastic processes on (101) planes arise in MD simulations already after time step 14000 (linear phase of loading, $\sigma_A \approx 2.04$ GPa) near the free sample surface. Analysis of atomic displacements below and above the slip band confirmed that the relative shear displacements correspond to the Burgers vector. The slip patterns along the crack front disappear at a certain distance from the free sample surface. This behavior is explained in Figure 5. The figure shows atomic configuration in two slip planes (101) containing the left crack front. The view (101)[101] (perpendicular to the slip plane) in Figure 5a illustrates that a curved dislocation has been emitted on the (101) plane from the corner where the left crack front penetrates the free sample surface. It is visible that the slip process disappears along the crack front at time step 14030 at a certain distance from the corner. Note that dislocation emission from the corner has been observed also in 3D crack simulations with an EAM Cu-potential [19]. Emission of the curved dislocation loop agrees with the expectation following from the continuum theory of dislocations, where curved dislocations loops have smaller strain energy in comparison with straight (line) dislocations. No shear processes are visible on {112} planes at time step 14030. Further time development is following: the dislocation loop on (101) plane expands under the shear stresses τ_b, $\sigma_{\theta r}$ (Figure 5b) and gradually changes its shape to a straight screw segments (Figure 5c) that can change the slip planes to {112}. It explains the second deviated slip patterns mentioned above. The slip stress τ_b (acting in the direction of the Burgers vector $\boldsymbol{b}$) and the shear stress $\sigma_{\theta r}$ derived [14] according to anisotropic [18] and isotropic LFM for the plane strain and plane stress conditions are given below:

plane strain {110} $\sigma_{\theta r} = 0.296\ K_I / (2\pi r)^{1/2}$ (0.327 ISO), $\tau_b = 0.242\ K_I / (2\pi r)^{1/2}$ (0.267 ISO),

{112} $\sigma_{\theta r} = 0.208\ K_I / (2\pi r)^{1/2}$ (0.218 ISO), $\tau_b = 0.184\ K_I / (2\pi r)^{1/2}$ (0.201 ISO),

plane stress {110} $\sigma_{\theta r} = 0.302\ K_I / (2\pi r)^{1/2}$ (0.327 ISO), $\tau_b = 0.246\ K_I / (2\pi r)^{1/2}$ (0.267 ISO),

{112} $\sigma_{\theta r} = 0.209\ K_I / (2\pi r)^{1/2}$ (0.218 ISO), $\tau_b = 0.366\ K_I / (2\pi r)^{1/2}$ (0.371 ISO).

It may be seen that larger stress intensity at the crack front can be expected near a free sample surface, where plane stress conditions must prevail in the normal direction. It explains why the slip processes start at the free sample surface.

The jogs in the crack front (Figure 4a) coming from the <111>{112} slip systems later cause a slow plastic crack growth in the middle of the crystal. Under the same conditions (time step and loading) the crack near the free sample surface remains stable since it is blunted by the previous dislocation emission on the inclined (101) planes (Figure 4b).

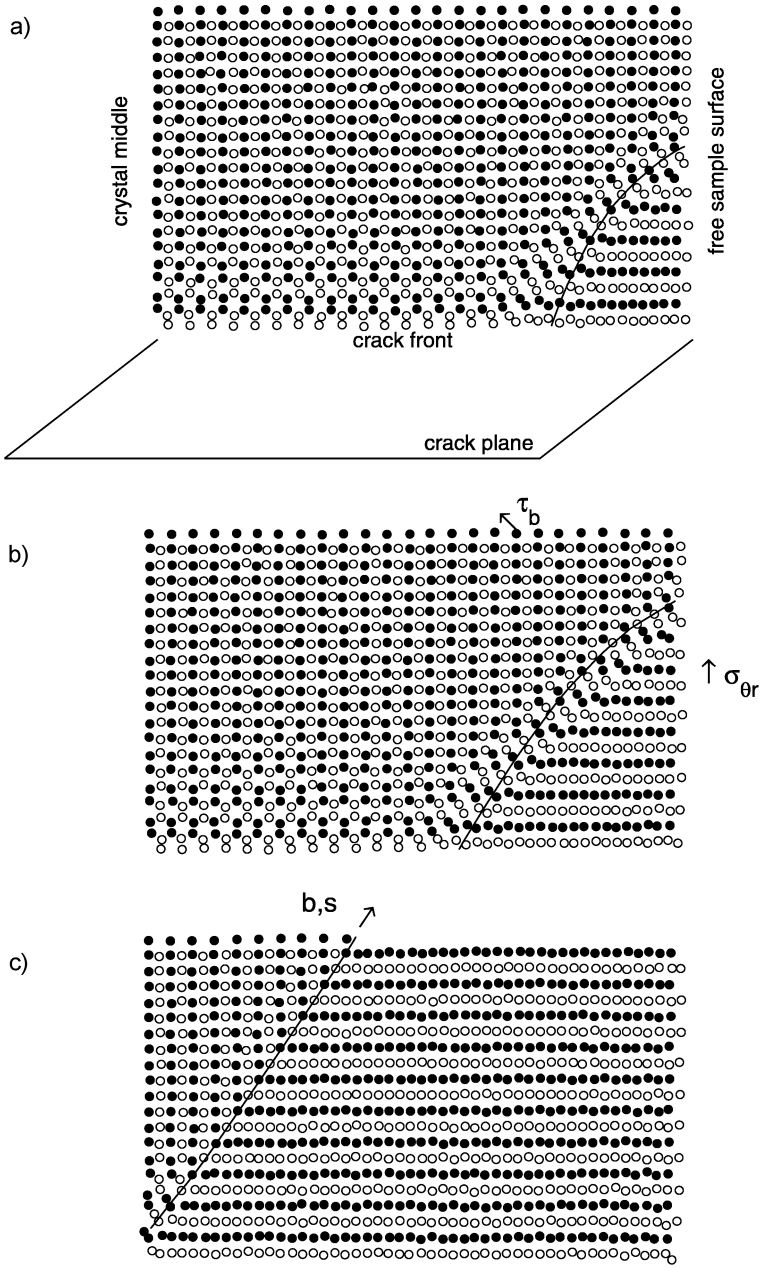

Figure 5. Slip patterns on two {101} planes for time step: a) 14030, b) 14100, c) 14670. 300 K, view (101)[101]. [14]

The critical shear stress needed for dislocation emission at temperature of 0 K on {112} planes is presented for our potential in [7]. The stress barrier corresponds to τ_{disl} = 16.3 GPa. The peak stress, i.e. the stress needed for dislocation emission on {110} planes is τ_{disl} = 14.5 GPa, as follows from our BLS simulations at 0 K. It may be seen that the stress barrier for dislocation emission with the used potential is smaller on {110} plane in comparison with {112} planes. It explains why dislocation generation in our MD simulations begins on {110} planes. As follows from [8], the stress barrier can be decreased by the presence of T-stress acting along crack plane. According to Rice [20], the critical shear stress in a slip plane inclined with respect to the crack plane under an angle θ is reduced via a simple interchange $\tau_c \rightarrow \tau_c + T \sin\theta \cos\theta$. For our large crystal, the boundary correction factor is $F_I \approx 1$ according to [21] and $T \approx -\sigma_A$. As mentioned above, the applied stress in MD at the time of dislocation generation corresponds to $\sigma_A \approx 2.04$ GPa. It decreases the stress barrier for dislocation emission on {110} planes at temperature 0 K by about 1 GPa to τ_{disl} = 13.5 GPa. As follows from [16], further reduction of the critical loading by about 10-15 % is expected due to tension-shear coupling, i.e. due to a small normal relaxation in the slip system.

The barrier should be smaller at elevated temperature of 300 K, since thermal atomic motion can assist dislocation generation [2].

Edge (001)[110] crack

In this case, the slip systems <111>{112} are inclined to the crack plane under the angle $\theta = 35.26^{o}$, contain the crack front and they are oriented in the easy twinning direction, similar to plane strain simulations [7]. As follows from [7], in this case the stress barrier for twin formation in the <111><112> slip systems at temperature of 0 K is much lower (τ_{twin} = 9.3 GPa) than for dislocation generation (16.3 GPa) with the used N-body potential.

Crack initiation has been monitored first in the middle of the sample at time step 3382 (σ_A = 6.27 GPa). Considering the flight time correction (759 time steps) and the boundary correction factor F_I = 1.27, it corresponds in MD to stress intensity at the crack front K_I = 0.749 MPa $m^{1/2}$. It is close to $K_{I\,c}$ = 0.835 MPa $m^{1/2}$ expected according to anisotropic LFM for plane stress and the used potential with the surface formation energy $2\gamma_{001}$ = 3.624 J/m^2**.**

Similar to plane strain simulations [7], crack initiation was accompanied by generation of unstable stacking faults that later transform to twins in the <111>{112} slip systems. Figure 6 shows twinning in the middle of the crystal at time step 3600, while Figure 7 shows the crack and twin surfaces in 3D. This figure was extracted from the output file according to local number of atomic interactions. Later (under higher applied loads), dislocation emission in the inclined slip system <111>{112} has been monitored at the crack front, leading to crack blunting and to de-twinning at the crack tip -see Figure 8 at time step 4100. As above, the emission of dislocations begins at the free sample surfaces. At time step 4200, the simulations were terminated to avoid plastic damage of the loaded borders.

Note that de-cohesion along twin-matrix interfaces or crack deflections into the <111>{112} slip systems were observed in 3D already before the dislocation emission during the twinning period. It is in a qualitative agreement with experimental observations in bcc iron, where fracture surface consists of {100} cleavage facets and {112} tongues.

Unlike our previous plane strain simulations at 0 K (e.g. in [7]), at temperature of 300 K twinning in 3D simulations is sensitive to loading rate - twins are observed only under faster loading. It complies with experimental observations, e.g. in [10].

Our results are also in a qualitative agreement with an experimental post-fracture SEM and TEM analysis, where twins and dislocations in the <111>{112} slip systems have been observed [22] below fracture surfaces in the Fe-Si(3wt%) single crystals under a faster loading (for cross head speed 1mm/min in [11]).

Due to finite geometry of the sample with edge crack, more convenient stress analysis is possible in the framework of isotropic LFM, where the T-stress for finite geometry is tabulated [23]. For our geometry (a/W = 0.3, (L/2)/W > 1.5), the T-stress is given by the relation $T = -0.5876\ \sigma_A$.

Twinning in MD occurred near the critical level of loading, where $\sigma_A = \sigma_{cr} = K_{I\,c} / F_I / (\pi l_o)^{1/2}$ = 4.76 GPa, corresponding T = -2.8 GPa and Rice correction is $T \sin\theta \cos\theta$ = -1.32 GPa. It decreases the stress barrier for twinning to τ_{twin} = 7.98 GPa. For our crack and slip geometry $\tau_b = \sigma_{\theta r} = 0.275\ K_I / (2\pi r)^{1/2}$ according to [1]. Taking the value $K_{I\,c}$ given above and the distance from the crack tip r = *b* / 2, we obtain $\sigma_{\theta r}$ = 8.2 GPa > τ_{twin}, i.e. twinning at the crack front is possible also according to LFM.

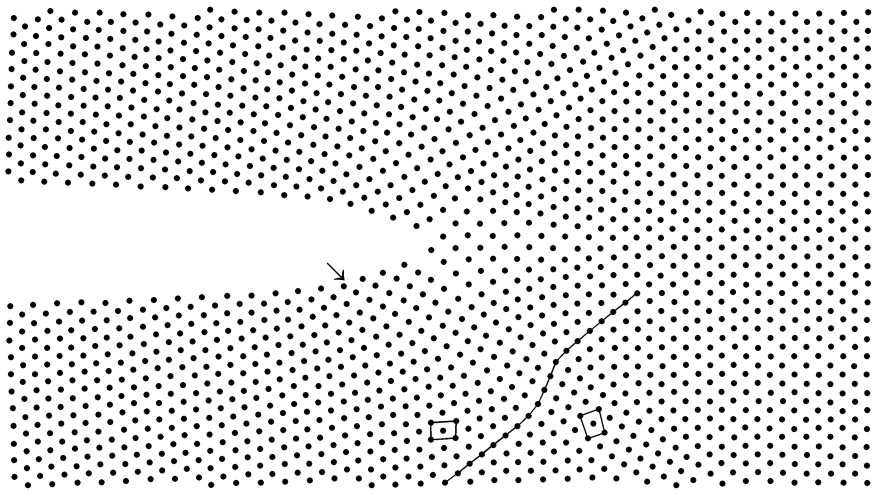

Figure 6. Twinning in the middle of the crystal, time step 3600. The arrow denotes the original crack tip point.

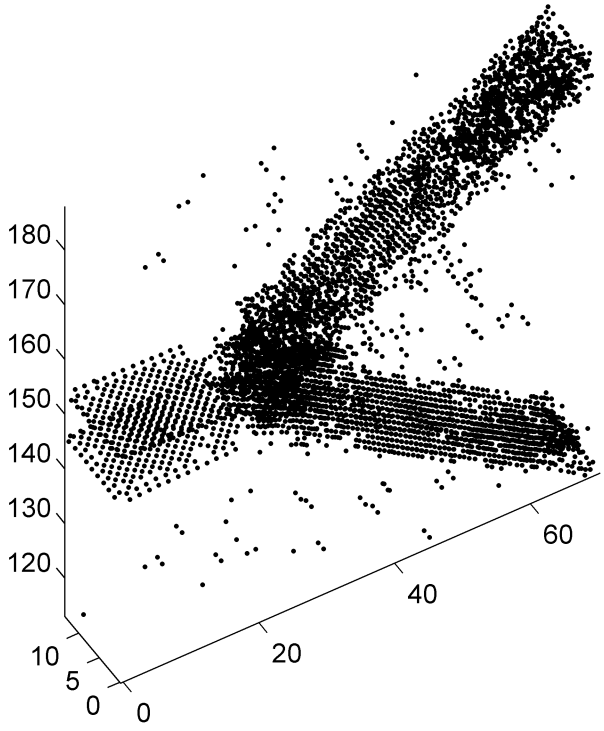

Figure 7. Crack (to the left) and twins (to the right) in 3D, time step 3600.

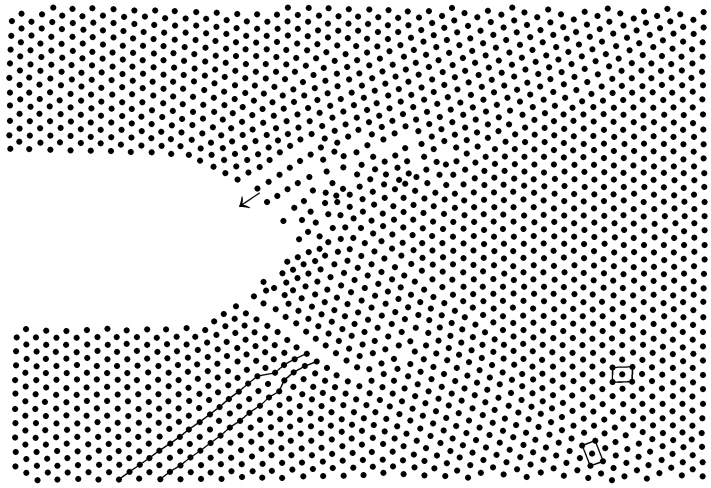

Figure 8. Dislocation emission below twin bands, time step 4100. The first (110) surface layer is shown.

As to dislocation emission in 3D continuum, Rice and Beltz in [2] analyzed influence of thermal activation on nucleation of a dislocation loop from the crack front loaded in mode II. According to [2], the energy needed for dislocation generation at room temperature in bcc iron could be $G \approx 0.8 - 0.9\ G_{crit}$, where $G_{crit} = \gamma_{us}$ is the energy needed for nucleation of a straight dislocation in mode II at temperature of 0 K. The unstable stacking fault energy with our potential in the slip system

<111>{112} is γ_{us} = 1.14 J/m^2 [7]. The energy needed for generation of a straight edge dislocation from the crack front loaded in mode I into the inclined slip system at temperature of 0 K is in our case $G_{disl} = 8\,\gamma_{us} / (1+\cos\theta)\,\sin^2\theta$ = 15.06 J/m^2 by Rice model [1]. Assuming that in mode I $G_{crit} = G_{disl}$ and G(300 K) = 0.8 G_{disl}, we obtain G(300 K) = 12.05 J/m^2 as a material parameter according to continuum. Dislocation emission in MD occurred at time step 4100, which corresponds to applied stress σ_A = 8.16 GPa and applied stress intensity $K_{MD} \approx F_I\,\sigma_A\,(\pi l)^{1/2}$ = 1.57 MPa m$^{1/2}$. It gives $G_{MD} = C\,K^2_{IMD}$ = 12.82 J/m^2, which exceeds the expected value of G(300 K), i.e. dislocation emission in MD at temperature of 300 K is possible also according to this continuum approximation. A further decrease in the energy needed for dislocation nucleation in the continuum model one can expect from the anisotropy, T-stress and normal relaxation in the slip system, as already discussed above.

Conclusions

For crack orientation (001)[010], we performed the 3D simulations at temperature of 0 K and 300 K. The samples were loaded in mode I slowly, gradually in time. While at the temperature of 0 K brittle crack initiation has been observed, at 300 K dislocation emission and slip processes on {110} and {112} planes have been detected. The slip processes start at the free sample surfaces, which is in a qualitative agreement with our stress analysis and MD simulations by Zhou et al. [19]. The process begins on {110} planes via emission of a curved dislocation (~ quarter circle loop) from the corners, where the crack penetrates the free sample surfaces. MD simulations further show that slip processes on the inclined {110} planes cause crack blunting and hinder crack growth. The slip processes on the oblique {112} planes make jogs in the crack front and enable a slow plastic crack growth. It could be a micromechanism for the plastically induced fracture reported in experiments on iron crystals of equivalent orientation by March *et al* [9].

The second crack orientation (001)[110] has been motivated by our fracture experiments [11] on Fe-Si(3wt%) single crystals with edge crack, performed at room temperature. Here the 3D-simulations at 300 K under a faster loading monitored crack initiation accompanied by twinning at the crack front and crack deflections into the <111>{112} slip systems along twin-matrix interfaces. It complies with experimental observations in bcc iron, where fracture surfaces consist of {100} cleavage facets and {112} tongues. Later (under higher loads), dislocation emission in the inclined <111>{112} slip systems has been monitored in MD, causing crack blunting and slower crack growth. MD results are in a qualitative agreement with post-fracture SEM and TEM analysis in [22], where twins and dislocations in the <111>{112} slip systems have been observed below fracture surfaces in the Fe-Si single crystals. Twinning at the crack tip may precede dislocation emission as well according to a new continuum model presented in [24].

Acknowledgments

The work was supported by the Grant Agency AS CR under grants IAA2076201 and AV0Z20760514.

References

1. Rice, J. R., “Dislocation Nucleation from a Crack Tip: an Analysis Based on the Peierls Concept”, J. Mech. Phys., 4**0**, 239-271 (1992).
2. Rice, J. R. and Beltz, G. E., “The Activation Energy for Dislocation Nucleation at a Crack”, J. Mech. Phys., **42**, 333-360 (1994).
3. Beltz, G. E. and Fisher, L. L., “Effect of T-Stress on Edge Dislocation Formation at a Crack Tip under Mode I Loading”, In: Multiscale Deformation and Fracture in Materials and Structures, (Boston, Kluwer, eds. T. J. Chuang and J. W. Rudnicki), 237-242 (2001).
4. Mullins, M. and Dokainish, M. A, “Simulation of the (001) crack in α-Iron Employing a New Boundary Scheme”, Phil. Mag. A, **46**, 771-787 (1982).
5. Kohlhoff, S., Gumbsch, P. and Fischmeister, H. F., "Crack Propagation in B.C.C Crystals Studied with a Combined Finite-Element and Atomistic Model", Phil. Mag. A, **64**, 851-878 (1991)
6. Shastry, V. and. Farkas D., “Molecular Statics Simulation of Fracture in α-Iron”, Modelling. Simul. Mater. Sci. Eng., **4**, 473-492 (1996)
7. Machová, A., Beltz, G. E., and Chang M., “Atomistic Simulations of Stacking Fault Formation in BCC Iron”, Modelling. Simul. Mater. Sci. Eng., **7**, 949-974 (1999)
8. Beltz, G. E. and Machová, A., “Effect of T-Stress on Dislocation Emission in Iron”, Scripta Materialia, **50**, 483-487 (2004).
9. Marsch, P. G., Zielinski, W., Huang, H. and Gerberich, W. W., "Crack-Tip Dislocation Emission Arrangements for Equilibrium- III. Application to Large Applied Stress Intensities", Acta mettal. mater., **40**, 2883-2894 (1992)
10. Šmida, T. and Bošanský, J., “Deformation Twinning and its Possible Influence on the Ductile-Brittle Transition Temperature of Ferritic Steels”, Mater. Sci. Eng. A, **287**, 107-115 (2000)

11. Landa, M., Machová, A., Převorovský, Z., Červ, J. and Adámek, J., "Crack growth in Single Crystals of α-Iron (3wt%Si)", Czech. J. Phys., **48**, 1589-1606 (1998)
12. Ackland, G. J., Bacon, D. J., Calder, A. F. and Harry, T., "Computer Simulation of Point Defect Properties in Dilute Fe-Cu Alloy Using a Many-Body Interatomic Potential", Phil. Mag. A, **75**, 713-732 (1997)
13. Machová, A., "Residual Stress in Fe-Cu Alloys at 0 and 600 K", Computational Materials Science, **24**, 535-543 (2002)
14. Pelikán, V.,Hora, P., Machová, A. and Spielmannová, A., "Brittle-Ductile Behavior in 3D Iron Crystals", Czech. J. Phys., **55**, xxxx-xxxx (2005), in press
15. Pokluda, J. and Šandera, P., "On the Intrinsic Brittleness and Ductility", Metallic Materials, **33**, 375-383 (1995)
16. Sun, Y. and Beltz, G. E., "Dislocation Nucleation from a Crack Tip: a Formulation Based on Anisotropic Elasticity", J. Mech. Phys. Solids, **42**, 1905-1932 (1994)
17. Dienes, G. J. and Paskin, A., "Molecular Dynamic Simulation of Crack Propagation", J. Phys. Chem. Solids, **48**, 1015-1033 (1987)
18. Tada, , Paris, P. and Irwin, G., "The Stress Analysis Handbook", Hellertown Del Research Corporation , Hellertown PA, D1-3 (1973)
19. Zhou, S.J., Beazley, D. M., Lomdahl, P.S., Voter, A.F. and Hollian, B.L., "Dislocation Emission from a Three - Dimensional Crack - a Large Scale Molecular Dynamic Study", In: Advances in Fracture Research (ICF9-Sydney, eds. B.L. Karihaloo *et al.*), 3085-3094, New York, Pergamon (1997)
20. Rice, J. R., "Limitations to the Small Scale Yielding Approximation for Crack Tip Plasticity", J. Mech. Phys. Solids, **22**, 17-26 (1974)
21. Murakami, Y. (ed.), "Stress Intensity Factors Handbook", Vol.1, 67-68, Pergamon, Oxford (1988)
22. Prahl, J., Machová, A., Landa, M., Haušild, P., Karlík, Clavel, M. and Haghi-Ashtiani, P., "Fracture of Fe-3%Si Single Crystals", 10th International Symposium on Physics of Materials, The Book of Abstracts, FMP Charles University, Prague 30.8.-2.9.2005, to appear in Mater. Sci. Eng. A
23. Fett, T., "A Compendium of T-stress Solutions", Research Report FZKA 6057, Forshungszentrum Karlsruhe GmbH, 1-72 (1998)
24. Beltz, G.E., Chang, M. and Machová A., "A Model for Crack Induced Nucleation of Dislocations, Complex Stacking Faults and Twins", In: Materials Structure & Micromechanics of Fracture (ed. J. Pokluda), Materials Science Forum, **482**, 17-24 (2005)